Revision 1

Hanswilkeite, $KFeS_2$, a new peralkaline sulfide mineral

Sergey N. Britvin[1,2]*, Mikhail N. Murashko[1], Maria G. Krzhizhanovskaya[1], Oleg S. Vereshchagin[1], Yevgeny Vapnik[3]*, Natalia S. Vlasenko[1], Yulia S. Shelukhina[1], and Vladimir N. Bocharov[1]

[1] Saint-Petersburg State University, Universitetskaya Nab. 7/9, 199034, St. Petersburg, Russia

[2] Kola Science Center, Russian Academy of Sciences, Fersman Str. 14, 184200, Apatity, Russia

[3] Department of Geological and Environmental Sciences, Ben-Gurion University of the Negev, P.O.B. 653, Beer-Sheva 84105, Israel

ABSTRACT

Hanswilkeite, $KFe^{3+}S_2$, is a new potassium-rich natural sulfide discovered in the pyrometamorphic suite of the Hatrurim Formation, southern Negev Desert, Dead Sea basin, Israel. The mineral occurs in sulfide-calcite assemblages confined to black-colored calcite-spurrite marbles. It forms single-crystal grains up to 1 mm in size, isometric to lath-like, often intergrown with a less-common rasvumite, KFe_2S_3. Associated minerals include srebrodolskite, tilleyite, fluormayenite, cuspidine, fluorapatite, oldhamite, pyrite, and andradite. Macroscopically, hanswilkeite has a deep-purple color, dull metallic luster and brown-black streak. The Mohs' hardness is 2. Moderate cleavage was observed along the *c*-axis. The calculated density is 2.654 $g \cdot cm^{-3}$. The Raman spectrum contains the following bands: 379, 357, 289, 236, 167, 131 and 124 cm^{-1}. In reflected light, the mineral has very strong pleochroism from yellow-pink to dark-grey. Anisotropy is very strong, ΔR_{589} = 69 %. Reflectance values for COM required wavelengths measured in air, R_{max}/R_{min} (λ, nm) (%): 16.0/9.2 (470); 19.6/9.3 (546); 18.5/9.0 (589); 32.0/9.3 (650). Chemical composition (electron microprobe, average of 6 points, wt. %): K 23.78, Ca 0.44, Fe 34.75, Mn 0.60, Zn 0.47, S 39.46, Total 99.5, that corresponds to empirical formula $(K_{0.98}Ca_{0.02})_{1.00}(Fe_{1.00}Mn_{0.02}Zn_{0.01})_{1.03}S_{1.98}$ (Σ = 4 *apfu*) or ideally $KFe^{3+}S_2$. Single-crystal X-ray diffraction study shows that the mineral is monoclinic, space group *C*2/*c* (#15), with unit-cell parameters *a* = 7.0914(5), *b* = 11.3154(5), *c* = 5.3992(3) Å, β = 113.244(7)°, *V* = 398.08(4) $Å^3$ and *Z* = 4. Strongest lines of X-ray powder diffraction pattern [*d* in Å(I)(*hkl*)]: 5.68(100)(020,110); 3.270(31)(130); 3.227(29)(111); 2.921(45)(–221); 2.510(12)(131); 2.198(12)(–132); 1.880(10)(330). The crystal structure has been solved and refined to R_1 = 0.038 for 454 unique observed reflections [$I \geq 2\sigma(I)$]. The structure consists of infinite chains of edge-sharing tetrahedra $[FeS_4]^-$ centered with Fe^{3+}; the sulfide chains are linked by K^+ ions. Hanswilkeite is the third discovered dithioferrate mineral: a sulfosalt that contains $[FeS_2]^-$ anion with iron in Fe^{3+} state. Other known natural dithioferrates are erdite, $NaFeS_2 \cdot 2H_2O$, and raguinite, $TlFeS_2$. Hanswilkeite has a synthetic counterpart and a group of

related synthetic sulfides and selenides, well studied due to specific electrical and magnetic properties owed to their quasi-one-dimensional structures. The mineral can be considered as an indicator of an extreme potassium-rich environment superimposed onto anhydrous and oxidizing formation conditions. The association with oldhamite is herein discussed in view of super-reduced conditions previously supposed for oldhamite geosynthesis.

Keywords: hanswilkeite, $KFeS_2$, rasvumite, oldhamite, peralkaline, potassium, marble, Hatrurim Formation

This is the peer-reviewed, final accepted version for American Mineralogist, published by the Mineralogical Society of America.
The published version is subject to change. Cite as Authors (Year) Title. American Mineralogist, in press.
DOI: https://doi.org/10.2138/am-2024-9494. http://www.minsocam.org/

INTRODUCTION

Potassium, being an alkali metal, expresses strong lithophile affinity both in Earth's crust and in extra-terrestrial matter (Oversby and Ringwood 1972; Christy 2018). The chalcophile behaviour of this element was fist encountered with a discovery of djerfisherite, supposedly $K_3(Na,Cu)(Fe,Ni)_{12}S_{14}$, in highly reduced assemblages of enstatite meteorites (Fuchs 1966). A few years later, djerfisherite was discovered on Earth (Sokolova et al. 1971). Since that, the mineral, currently defined as a mixed sulfide-chloride $K_6(Fe,Cu,Ni)_{25}S_{26}Cl$, was recognized to be characteristic for several meteorite groups (e.g., El Goresy et al. 1971; Clay et al. 2014; Lorenz et al. 2020; Sharygin 2022). What is more important, djerfisherite and some of its structural relatives were found to be dominant carriers of chalcophile potassium in the lithosphere: in mafic and ultramafaic rocks of mantle origin (e.g., Morgan et al. 1985; Sharygin et al. 2008; Barkov et al. 2015; Abersteiner et al. 2019), inclusions in diamonds (e.g., Bulanova et al. 1980; Hunt et al. 2012); alkaline mafic rocks and carbonatites (e.g., Sokolova et al. 1971; Yakovenchuk et al. 2003; Clay et al. 2014; Panina and Isakova 2019; Sorokhtina et al. 2019), metamorphic and pyrometamorphic complexes (e.g., Sokol et al. 2019). The essential, albeit minor constituent of djerfisherite is chlorine, and only in the absence of it, ternary potassium-iron-sulfide minerals can be formed. These are bartonite, $K_6Fe_{20}S_{27}$ and gmalimite, $K_6\square Fe_{24}S_{27}$ – both are structural derivatives of djerfisherite (Czamanske et al. 1979, 1981; Galuskina et al. 2019), and structurally distinct rasvumite, KFe_2S_3 (Sokolova et al. 1970). The occurrence of chlorine-free potassium iron sulfides is the same as of djerfisherite (e.g., Sharygin et al. 2007; Chakhmouradian et al. 2007; Barkov et al. 2015; Sokol et al. 2019), but they are noticeably rarer. Rasvumite, having an atomic ratio K/Fe = 1/2, was, until now, the potassium-richest iron sulfide mineral, although much more potassic compounds exist in the system K–Fe–S (Osadchii et al. 2018). In this paper, we report the discovery of $KFeS_2$, the first natural potassium-bearing dithioferrate: the sulfosalt of the $[FeS_2]^-$ anion where, in contrast to other natural K–Fe sulfides, all iron is comprised by Fe^{3+}. The synthetic analogue of the reported new mineral, hanswilkeite, is

potassium dithioferrate (III), a readily preparable compound, which is well studied due to its unusual electrical and magnetic properties determined by its quasi-one-dimensional chain structure (e.g., Bronger et al. 1987; Li et al. 2021). Why $KFeS_2$ has not yet been encountered in nature is seemingly due to a combination of the specific oxidative and hyperalkaline environment needed for its formation – which are rarely encountered together in nature. We herein discuss the occurrence of natural $KFeS_2$ and its association with oldhamite, CaS, the latter being usually considered as an indicator of a highly reduced environment.

The new mineral is named in honour of Dr. Hans-Jürgen Wilke (1925–2014), the German mineral collector, for his contributions to popularisation of mineralogy (e.g., Wilke 1976, 1997). Both the mineral and its name have been approved by the Commission on New Minerals, Nomenclature and Classification, International Mineralogical Association (IMA 2022-041). The holotype specimen of hanswilkeite is deposited in the collections of the Fersman Mineralogical Museum, Russian Academy of Sciences, Moscow, Russia, with the registration number 5862/1.

SAMPLES AND METHODS

It was found that hanswilkeite and associated oldhamite are moisture-sensitive minerals. Hanswilkeite, while exposed onto the sample surface at room humidity, becomes rusty within 1-2 days. The reason for such behaviour is unclear, because synthetic $KFeS_2$ was found to be quite stable in an aquatic environment (Osadchii et al. 2018). It is possible that oxidation of hanswilkeite is triggered by some reactions at the contacts with associated minerals. Oldhamite, at the same conditions, completely decomposes into a mixture of portlandite and unidentified amorphous carbonates and sulfur-containing calcium compounds. To prevent hydrolytic alteration of both sulfides, polished sections intended for the study were prepared avoiding water, using dry abrasives and hexane, and were stored in hexane until and after analytical procedures. ***Reflectance spectra*** were recorded with a POLAM P-312 microscope equipped with a MSFP microspectrophotometer

This is the peer-reviewed, final accepted version for American Mineralogist, published by the Mineralogical Society of America.
The published version is subject to change. Cite as Authors (Year) Title. American Mineralogist, in press.
DOI: https://doi.org/10.2138/am-2024-9494. http://www.minsocam.org/

(LOMO, St. Petersburg). The spectra were measured in air using a Si standard. ***Electron microprobe data*** were obtained by means of an Oxford Instruments AzTec Energy X-Max 20 EDX spectrometer using an accelerating voltage of 20 kV and a current 1 nA, attached to a Hitachi S-3400N SEM. The WDX spectrometers were not used because it was found that hanswilkeite decomposes (looses potassium) under the beam current required for WDX analysis. The following reference standards were used: microcline (K-*K* series), chkalovite (Na-*K*), diopside (Ca-*K*), pyrite (Fe-*K*, S-*K*), $MnCO_3$ (Mn-*K*), ZnS (Zn-*K*,*L*), $Rb_2Nb_4O_{11}$ (Rb-*L*), with matrix correction by the extended Pouchou and Pichoir (XPP) method (Pouchou and Pichoir 1991). ***Powder X-ray diffraction*** data were obtained by the use of a Rigaku RAXIS Rapid II diffractometer. The instrument is equipped with a Co*K*α rotating anode operated at 40 kV and 15 mA, microfocus mirror monochromator and semi-cylindrical imaging plate detector (r = 127.4 mm). The images were acquired in Debye-Scherrer geometry from the grains powdered in oil; exposure time 60 min. An image-to-profile data conversion was performed using osc2xrd program (Britvin et al. 2017). Further processing of the pattern was carried out with Stoe WinXPOW v. 2.03 package (Stoe and Cie GmbH). ***Single-crystal X-ray diffraction*** data collection was carried out on a crystal fragment handpicked from a calcite nest, by means of a Rigaku Oxford Diffraction XtaLAB Synergy-S diffractometer equipped with a microfocus X-ray tube (Mo*K*α) and HyPix-6000 hybrid photon counting detector. Data collection and reduction procedures were performed using CrysAlisPro software (Rigaku Oxford Diffraction). The crystal structure has been solved and refined using the *SHELX*-2018 set of programs (Sheldrick 2015) incorporated into Olex2 GUI (Dolomanov et al. 2009). The details of data collection and structure refinement can be retrieved from the CIF file included into Supplementary Data. ***Raman spectroscopy.*** The Raman spectrum of hanswilkeite was recorded from a polished section by means of a Horiba Jobin-Yvon LabRam HR800 spectrometer operated with a green diode laser (λ = 532 nm, power 15 mWt), and an Olympus BX41 microscope, using a 50× confocal objective.

RESULTS AND DISCUSSION

Occurrence, appearance and mineral assemblages

Hanswilkeite was discovered within the rocks of the Hatrurim Formation – a large pyrometamorphic complex whose outcrops are traced across the area of 150×200 km^2, surrounding the Dead Sea basin in Israel, Palestine Authority and Jordan. There is a sufficient volume of a literature devoted to the Hatrurim Formation, where the readers can view the overall picture and details of pyrometamorphic processes which have had take place in this part of the Middle East several million years ago (Gross 1977; Burg et al. 1992; Vapnik et al. 2007; Novikov et al. 2013; Britvin et al. 2023). In the context of the present paper, it is important that pyrometamorphism has resulted in rather wide range of temperatures (from ambient to 1400 °C) and led to extreme spatial inhomogeneity of redox environments. This unique combination of conditions allowed the formation of both highly reduced assemblages, such as phosphides and nitrides (Britvin et al. 2021a,b, 2022; Galuskin et al. 2022), along with those which approach the oxidative limit accessible in nature, like chromate $(CrO_4)^{2-}$ and selenate $(SeO_4)^{2-}$ bearing minerals (e.g., Juroszek et al. 2020).

The most ubiquitous lithologies in the Hatrurim Formation are the marbles, whose varicoloured palette defines yet another of Hatrurim's traditional names – "the Mottled Zone" (Gross 1970). The local marbles have been furnished as ornamental stone since the Neolithic (Wright et al. 2008). Hanswilkeite was discovered in a small, now abandoned quarry formerly operated for ornamental stone. The quarry, 31°11'10"N, 35°15'37"E, is situated ~8 km to the west of Ein-Bokek (Israel coast of the southern sub-basin of the Dead Sea) and ~500 m to the east of Nahal Gorer (wadi Gorer) in the Hatrurim Basin, Negev desert, Israel. The quarry exposes a diversity of marble lithologies. Hanswilkeite-bearing marbles are dense, microcrystalline rocks that are black in color on freshly cleaved surfaces, that become tan-colored upon weathering (Figure 1a). The thickness of marble beds reaches 4-5 meters. The dominant constituents of the marble, given by powder XRD analysis, are calcite (~90%) and spurrite, $Ca_5(SiO_4)_2(CO_3)$. The main accessory phase

This is the peer-reviewed, final accepted version for American Mineralogist, published by the Mineralogical Society of America.
The published version is subject to change. Cite as Authors (Year) Title. American Mineralogist, in press.
DOI: https://doi.org/10.2138/am-2024-9494. http://www.minsocam.org/

147 is srebrodolskite $Ca_2(Fe^{3+},Al)_2O_5$, which imparts black color to the marble (Figure 1b). Other
148 accessory phases are tilleyite, $Ca_5(Si_2O_7)(CO_3)_2$, fluormayenite, $Ca_{12}Al_{14}O_{32}F_2$, cuspidine,
149 $Ca_8(Si_2O_7)_2F_4$, andradite and fluorapatite. The marble blocks are usually dissected by white veinlets
150 composed of calcite and jennite, $Ca_9(Si_3O_9)_2(OH)_8 \cdot 8H_2O$ (Figure 1b). Hanswilkeite was found in the
151 late millimeter-sized calcite nests which appear as grey cloudy patches within the black marble
152 matrix (Figure 1b). The mineral occurs as segregations of minute lath-like crystals within calcite,
153 and small nests up to 0.2 mm infilling the interstices between calcite crystals (Figure 2a,b).
154 Associated minerals are oldhamite CaS, pyrite and srebrodolskite (Figure 2c,d). In one case, a
155 millimeter-sized grain of hanswilkeite, ovoidal in shape, has been found. In this grain, the mineral
156 has a quasi-single-crystal texture, and contains numerous, micrometer-sized, and evidently syntactic
157 intergrowths of rasvumite, KFe_2S_3 (Figure 3a,b). It should be emphasized that all minerals in
158 hanswilkeite-bearing assemblages are anhydrous phases. The exception is portlandite, $Ca(OH)_2$,
159 which is a product of secondary (even laboratory) alteration of oldhamite grains.
160

161 **Physical and optical properties**

162 Hanswilkeite, when exposed on a freshly broken marble surface, has a deep-purple color
163 with a dull metallic lustre, resembling potassium permanganate, $KMnO_4$ in appearance. It has a
164 brown-black streak. The Mohs' hardness is 2, and it is brittle. A moderate cleavage was observed
165 along the *c*-axis (coincident with the laths' elongation), but the number and indexes of cleavage
166 planes could not be determined. The density, 2.654 $g \cdot cm^{-3}$, was calculated based on empirical
167 formula and unit-cell parameters refined from single-crystal data. In polished sections, using a
168 polarizing microscope in reflected light, hanswilkeite exhibits extreme pleochroism, varying in color
169 from yellowish-pink to dull-grey. Internal reflections were not observed. In crossed nicols,
170 hanswilkeite shows a strong birefringence and very strong anisotropy (ΔR_{589} = 69 %), changing in
171 color from flame-purple-red to pale-purple (Figure 2a,b; 3a,b). Owing to its specific optical

properties, hanswilkeite is readily distinguished from associated bluish-grey to white rasvumite, even in intimate intergrowths (Figure 3b). It is noteworthy that the reflectance curves of hanswilkeite (Table 1, Figure 3c) show a remarkable, almost indistinguishable similarity with the reflectance spectra of another alkali dithioferrate mineral, erdite $NaFeS_2 \cdot 2H_2O$ (Czamanske et al. 1980). This suggests that specific optical characteristics of both minerals are caused by the presence of the common structural unit – infinite chains of $[Fe^{3+}S_4]$ tetrahedra (see the Crystal structure section).

Chemical composition

The mineral, when analysed in the properly prepared polished sections (see Samples and methods), has a uniform chemical composition, with no zoning, and shows only subordinate substitutions of K for Ca and Fe for Mn and Zn, respectively (Table 2). The analytical totals, being close to 100 %, evidence for the absence of water in the mineral composition. Recalculation of the average of 6 microprobe analyses leads to the empirical formula $(K_{0.98}Ca_{0.02})_{1.01}(Fe_{1.00}Mn_{0.02}Zn_{0.01})_{1.03}S_{1.98}$, based on 4 atoms per formula unit (*apfu*), or ideally, $KFe^{3+}S_2$. The similar calculations for associated rasvumite (Table 2) give the empirical formula $(K_{1.01}Ca_{0.05})_{1.06}(Fe_{1.97}Zn_{0.01})_{1.98}S_{2.95}$ (6 *apfu*). Hanswilkeite is the third natural dithioferrate – sulfosalt that contains the $[FeS_2]^-$ anionic unit that counter-balances the positive charges of metal ions. Its closest chemical and structural relatives are erdite, $NaFeS_2 \cdot 2H_2O$, which was discovered among alkaline sulfide associations of Coyote Peak, California (Konnert and Evans 1980), and raguinite, $TlFeS_2$, from thallium-bearing assemblages of the Allchar deposit, North Macedonia (Laurent et al. 1969; Klepp and Boller 1979).

This is the peer-reviewed, final accepted version for American Mineralogist, published by the Mineralogical Society of America.
The published version is subject to change. Cite as Authors (Year) Title. American Mineralogist, in press.
DOI: https://doi.org/10.2138/am-2024-9494. http://www.minsocam.org/

197 **Raman spectroscopy**

198 The Raman spectrum of hanswilkeite (Figure 4) contains the following bands (cm^{-1}): 379,
199 357 (stretching vibrations Fe–S in FeS_4 tetrahedra); 289 (bending modes in FeS_4 tetrahedra); 236,
200 167, 131 and 124 (lattice modes). These band assignments were made by analogy with the Raman
201 spectrum of raguinite, $TlFeS_2$ (Makreski et al. 2014). The spectrum of hanswilkeite contains no
202 bands in the O–H stretching or H_2O-bending regions, further evidence for the absence of hydroxyl
203 groups and molecular water in its composition. It is noteworthy that the Raman spectrum of
204 hanswilkeite is completely different from the spectra of the structurally related erdite, which are
205 provided in the RRUFF database (Lafuente et al. 2015), entry R070139. The reasons for these
206 differences are unclear; but we would like to note that both erdite spectra given in the RRUFF
207 database, currently, also differ from each other.

208

209 **X-ray diffraction and crystal structure**

210 Hanswilkeite is monoclinic, space group *C*2/*c* (#15). The unit-cell parameters refined from
211 the single-crystal data are: a = 7.0914(5), b = 11.3154(5), c = 5.3992(3) Å, β = 113.244(7)°, V =
212 398.08(4) $Å^3$ and Z = 4. The parameters refined on the basis of powder X-ray diffraction pattern
213 (Table 3) are consistent with the those from single-crystal data: a = 7.0846(5), b = 11.3234(8), c =
214 5.4069(4) Å, β = 113.189(6)°, V = 398.71(4) $Å^3$. The crystal structure, solved and refined to R_1 =
215 0.0383 based on 454 unique observed reflections [$I \geq 2\sigma(I)$], consists of infinite chains of edge-
216 sharing tetrahedra [FeS_4] that propagate along the *c*-axis (Figure 5), which results in the
217 stoichiometry corresponding to $[FeS_2]^-$, known as the dithioferrate (III), or dithioferrite anion (Boon
218 and MacGillavry 1942). The average Fe–S bond distance is 2.235 Å (Table 4). The connections
219 between parallel chains are realized through the K–S bonds (<K–S> = 3.39 Å). Because tetrahedral
220 chains in the structure are separated by K^+ ions (the interchain Fe–Fe distance is 6.68 Å), each chain
221 can be regarded as a one-dimensional electrical conductor, where the electronic transport is realized

222 via intrachain Fe–Fe interactions (Fe–Fe = 2.70 Å). Owing to this structural feature, $KFeS_2$, a
223 synthetic analogue of hanswilkeite, is known as a quasi-one-dimensional conductor and
224 antiferromagnetic material, a parent compound for a family of magnetic dithio- and diselenoferrates
225 of alkali metals (e.g., Bronger et al. 1987; Li et al. 2021). $KFeS_2$ is attractive from the viewpoint of
226 practical applicability, because it is readily synthesized in good crystals, is stable in aquatic
227 environment and, contrary to $TlFeS_2$, it is non-toxic. Among the minerals, the same chain geometry
228 is realized in erdite, $NaFeS_2 \cdot 2H_2O$ (Konnert and Evans 1980), and raguinite, $TlFeS_2$ (Klepp and
229 Boller 1979) (Figure 6, Table 5). The structural homologues of hanswilkeite are rasvumite, KFe_2S_3
230 (Clark and Brown 1980) with isostructural pautovite, $CsFe_2S_3$ (Pekov et al. 2005), and picotpaulite,
231 $TlFe_2S_3$ (Johan et al. 1970; Balić-Žunić et al. 2008). The comparison of the crystal structures of
232 hanswilkeite and rasvumite is provided in Figure 6. It can be seen that the structures are very
233 similar, but rasvumite contains infinite ribbons $[Fe_2S_6]^{\infty}$ composed of doubled edge-sharing
234 tetrahedra $[FeS_4]$. The latter results in a mixed-valent, Fe^{3+}/Fe^{2+} iron in rasvumite, whereas in
235 hanswilkeite, the iron is purely Fe^{3+}.
236 The similarity of the structures of hanswilkeite and rasvumite results in almost identical atomic
237 arrangements along the *b*- and *c*-axes (Figure 6) and in the same unit-cell parameters values along
238 these directions (Table 5). The latter explains why hanswilkeite and rasvumite readily form syntactic
239 intergrowths in the studied assemblages (Figure 3b).
240

241 **IMPLICATIONS**

242 The discovery of $KFeS_2$ in nature is interesting from several geological viewpoints. With the
243 atomic K/Fe ratio = 1, hanswilkeite is the most potassium-rich mineral in the K–Fe–S system. Until
244 now, the uppermost limit, with K/Fe = 1/2, was observed in rasvumite, KFe_2S_3. The latter is a
245 characteristic mineral of agpaitic assemblages in intrusive and effusive alkali mafic complexes:
246 Khibiny and Lovozero at the Kola Peninsula, Russia (Sokolova et al. 1970; Ifantopulo et al. 1983;

Lisitsin et al. 2002); Mont St. Hilaire, Quebec, Canada (Chakhmouradian et al. 2007); Coyote Peak, California (Czamanske et al. 1979); Point of Rocks, New Mexico (DeMark 1984); Oldoinyo Lengai, Tanzania (Jago and Gittins 1999; Mitchell 2006). In addition, rasvumite has been encountered in contact skarns (Jamtveit et al. 1997), pyrometamorphic rocks (Sokol et al. 2019), kimberlites (Sharygin et al. 2008) and even as inclusions in diamond, where Logvinova and Sharygin (2023) had erroneously misidentified rasvumite for hanswilkeite. None of the cited works (except for the last erroneous report) consider the possibility of $KFeS_2$ formation. In a study of phase equilibria in the system $KFeS_2$–Fe–S, Osadchii et al. (2018) compare several scenarios for $KFeS_2$ geosynthesis, where the most likely pathways require "either extremely high potassium activity or high sulfur fugacity sufficient for pyrite stability". It is noteworthy that hanswilkeite mineral associations described in this paper (Figure 2, 3) involve a $KFeS_2$–rasvumite–pyrite assemblage obtained by Osadchii et al. (2018). From the more global viewpoint, the existence of hanswilkeite substantially expands the upper limit of potassium alkalinity reachable in the natural system K–Fe–S. Taking into account the identification of rasvumite in several reduced, Martian meteorites (Ling and Wang 2015; García-Florentino et al. 2021), this might have implications not only to terrestrial but to Martian mineralogy as well.

Another implication of the hanswilkeite discovery is related to its coexistence with oldhamite, CaS, and srebrodolskite, $Ca_2(Fe^{3+},Al)_2O_5$ (Figure 2c). Oldhamite is a typical accessory phase in highly reduced meteorites – enstatite chondrites and enstatite achondrites (aubrites). It has also been reported from several other classes of reduced meteorites (e.g., Haberle and Garvie 2017). The origin of meteoritic oldhamite is still a matter of debate (e.g., Dai et al. 2024), but its association with native iron and silicides (perryite), as well as presence of Sm^{2+} and Yb^{2+} anomalies (Hammouda et al. 2024) evidence that oldhamite, at least in enstatite meteorites, was formed under extremely reduced conditions. The above mentioned djerfisherite, $K_6(Fe,Cu,Ni)_{25}S_{26}Cl$, is another common constituent of meteoritic oldhamite assemblages (e.g., Clay et al. 2014), and it expectedly

contains iron in Fe^{2+} state. Until the last decade, oldhamite on Earth was only known as a semi-anthropogenic product in burnt coal dumps (e.g., Chesnokov and Shcherbakov 1991), where the expected redox environment (oxygen fugacity) was approaching values that existed during the formation of enstatite meteorites. Therefore, both modes of occurrence of oldhamite have led to an opinion that this mineral is an univocal indicator of super-reduced formation conditions (e.g., Liu et al. 2023; Nestola 2023).

The first (and still the only known) findings of non-anthropogenic terrestrial oldhamite were reported recently in the Hatrurim Formation (Galuskin et al. 2013; Galuskina et al. 2017; Vereshchagin et al. 2024), including the hanswilkeite locality. It is important to note that oldhamite, in our case, coexists with hanswilkeite, a Fe^{3+} bearing sulfide, and even with srebrodolskite, a Fe^{3+}-rich oxide (Figure 2c). It appears improbable that mineral assemblages containing Fe^{3+}-bearing oxides and sulfides could form at an oxygen fugacity below the iron-wustite, Fe^{0}-FeO buffer – the redox environment associated with oldhamite formation. The simple and obvious consequence from the above observations is that the presence of oldhamite in natural mineral assemblages does not necessarily implies a super-reduced formation environment, as it was invoked in the cited works. Alternatively, the relatively low formation temperature expected for $KFeS_2$-rasvumite-pyrite assemblages (lower than 513 °C, according to the data reported by Osadchii et al. 2018) might result in kinetic "freezing" of redox reactions between the already formed hanswilkeite and srebrodolskite, from one side, and oldhamite, provided that the latter had formed at even lower temperature. This scenario is not improbable, considering the extreme thermal and redox inhomogeneities typical of the rocks of the Hatrurim Formation.

Acknowledgments

This study was funded by Russian Science Foundation, grant 24-17-00228. The authors gratefully acknowledge the anonymous referees for valuable comments and suggestions, and

297 Associate Editor Fabrizio Nestola for editorial handling of the manuscript. The studies were carried
298 out with instrumental and computational support of Resource Centre for X-ray Diffraction Studies
299 and Geomodel Resource Centre of St. Petersburg State University.

300

301 **References cited**

302 Abersteiner, A., Kamenetsky, V.S., Goemann, K., Golovin, A.V., Sharygin, I.S., Giuliani, A.,
303 Rodemann, T., Spetsius, Z.V., and Kamenetsky, M. (2019) Djerfisherite in kimberlites and
304 their xenoliths: implications for kimberlite melt evolution. Contributions to Mineralogy and
305 Petrology, 174, 1–22.
306 Balić-Žunić, T., Karanović, L., and Poleti D. (2008) Crystal structure of picotpaulite, $TlFe_2S_3$, from
307 Allchar, FYR Macedonia. Acta Chimica Slovenica, 55, 801–809.
308 Barkov, A.Y., Martin, R.F., and Cabri, L.J. (2015) Rare sulfides enriched in K, Tl and Pb from the
309 Noril'sk and Salmagorsky complexes, Russia: new data and implications. Mineralogical
310 Magazine, 79, 799–808.
311 Boon, J.W., and MacGillavry, C.H. (1942) The crystal structure of potassium thioferrite $KFeS_2$ and
312 sodium thiochromite $NaCrS_2$. Recueil des Travaux chimiques des Pays-Bas, 61, 910–920.
313 Britvin, S.N., Dolivo-Dobrovolsky, D.V., and Krzhizhanovskaya, M.G. (2017) Software for
314 processing the X-ray powder diffraction data obtained from the curved image plate detector of
315 Rigaku RAXIS Rapid II diffractometer. Zapiski Rossiyskogo Mineralalogicheskogo
316 Obshchestva, 146, 104–107 (in Russian).
317 Britvin, S.N., Vereshchagin, O.S., Shilovskikh, V.V., Krzhizhanovskaya, M.G., Gorelova, L.A.,
318 Vlasenko, N.S., Pakhomova, A.S., Zaitsev, A.N., Zolotarev, A.A., Bykov, M., Lozhkin, M.S.,
319 and Nestola, F. (2021a) Discovery of terrestrial allabogdanite $(Fe,Ni)_2P$, and the effect of Ni

and Mo substitution on the barringerite-allabogdanite high-pressure transition. American Mineralogist, 106, 944–952.

Britvin, S.N., Krzhizhanovskaya, M.G., Zolotarev, A.A., Gorelova, L.A., Obolonskaya, E.V., Vlasenko, N.S., Shilovskikh, V.V., and Murashko, M.N. (2021b) Crystal chemistry of schreibersite, $(Fe,Ni)_3P$. American Mineralogist, 106, 1520–1529.

Britvin, S.N., Murashko, M.N., Vapnik, Y., Zaitsev, A.N., Shilovskikh, V.V., Krzhizhanovskaya, M.G., Gorelova, L.A., Vereshchagin, O.S., Vasilev, E.A., and Vlasenko, N.S. (2022) Orishchinite a new terrestrial phosphide, the Ni-dominant analogue of allabogdanite. Mineralogy and Petrology, 116, 369–378.

Britvin, S.N., Murashko, M.N., Krzhizhanovskaya, M.G., Vapnik, Ye., Vlasenko, N.S., Vereshchagin, O.S., Pankin, D.V., Zaitsev, A.N., and Zolotarev, A.A. (2023) Yakubovichite, $CaNi_2Fe^{3+}(PO_4)_3$, a new nickel phosphate mineral of non-meteoritic origin. American Mineralogist, 108, 2142–2150.

Bronger, W., Kyas, A., and Muller, P. (1987) The antiferromagnetic structures of $KFeS_2$, $RbFeS_2$, $KFeSe_2$, and $RbFeSe_2$ and the correlation between magnetic moments and crystal field calculations. Journal of Solid State Chemistry, 70, 262–270.

Bulanova, G.P., Shestakova, O.E., and Leskova, N.V. (1980) Djerfisherite from sulfide inclusions in diamonds. Doklady Akademii Nauk SSSR, 255 (2), 430–433.

Burg, A., Starinsky, A., Bartov, Y., and Kolodny, Y. (1992) Geology of the Hatrurim Formation ("Mottled Zone") in the Hatrurim Basin. Israel Journal of Earth Sciences, 40, 107–124.

Chakhmouradian, A.R., Halden, N.M., Mitchell, R.H., and Horvath, L. (2007) Rb-Cs rich rasvumite and sector-zoned "loparite-(Ce)" from Mont Saint-Hilaire (Quebec, Canada) and their petrologic significance. European Journal of Mineralogy, 19, 533–546.

Chesnokov, B.V., and Shcherbakov, E.P. (1991) Mineralogy of burnt dumps of the Chelyabinsk coal basin. Moscow, Nauka, 152 p. (in Russian).

Christy, A.G. (2018) Quantifying lithophilicity, chalcophilicity and siderophilicity. European Journal of Mineralogy, 30, 193–204.

Clay, P.L., O'Driscoll, B., Upton, B.G.J., and Busemann, H. (2014) Characteristics of djerfisherite from fluid-rich, metasomatized alkaline intrusive environments and anhydrous enstatite chondrites and achondrites. American Mineralogist, 99, 1683–1693.

Clark, J.R., and Brown, G.E. (1980) Crystal structure of rasvumite, KFe_2S_3. American Mineralogist, 65, 477–482.

Czamanske, G.K., Erd, R.C., Sokolova, M.N., Dobrovol'skaya, M.G., and Dmitrieva, M.T. (1979) New data on rasvumite and djerfisherite. American Mineralogist, 64, 776–778.

Czamanske, G.K., Leonard, B.F., and Clark, J.R. (1980) Erdite, a new hydrated sodium iron sulfide mineral. American Mineralogist, 65, 509–515.

Czamanske, G.K., Erd, R.C., Leonard, B.F., and Clark, J.R. (1981) Bartonite, a new potassium iron sulfide mineral. American Mineralogist, 66, 369–375.

Dai, W., Moynier, F., and Siebert, J. (2024) Insights on the origin of oldhamite in enstatite meteorites from Ca stable isotopes. Geochimica et Cosmochimica Acta, 375, 247–257.

DeMark, R.S. (1984) Minerals of Point of Rocks, New Mexico. Mineralogical Record, 15, 149–156.

Dolomanov, O.V., Bourhis, L.J., Gildea, R.J., Howard, J.A., and Puschmann, H. (2009) OLEX2: a complete structure solution, refinement and analysis program. Journal of Applied Crystallography, 42, 339–341.

Dowty, E. (2006). ATOMS for Windows. Shape Software, Kingsport, Tennessee, USA.

El Goresy, A., Grögler, N., and Ottermann, J. (1971) Djerfisherite composition in Bishopville, Pena Blanca Springs, St. Marks and Toluca meteorites. Chemie der Erde, 30, 77–82.

Fuchs, L.H. (1966) Djerfisherite, alkali copper-iron sulfide: a new mineral from enstatite chondrites. Science, 153 (3732), 166–167.

Galuskin, E., Galuskina, I., Vapnik, Ye., Murashko, M., Prusik, K. and Dzierżanowski, P. (2013) Oldhamite CaS and potentially new mineral $CaCu_2S_2$ from pyrometamorphic rock of the Hatrurim formation. Goldschmidt 2013, Conference Abstracts, Mineralogical Magazine, 77, 1134.

Galuskin, E., Galuskina, I.O., Kamenetsky, V., Vapnik, Ye., Kusz, J., Zieliński, G. (2022) First In Situ Terrestrial Osbornite (TiN) in the Pyrometamorphic Hatrurim Complex, Israel. Lithosphere, 2022, 8127747.

Galuskina, I.O., Galuskin, E.V., Prusik, K., Vapnik, Y., Juroszek, R., Jeżak, L., and Murashko, M. (2017) Dzierżanowskite, $CaCu_2S_2$ – A new natural thiocuprate from Jabel Harmun, Judean Desert, Palestine Autonomy, Israel. Mineralogical Magazine, 81, 777–789.

Galuskina, I.O., Krüger, B., Galuskin, E.V., Krüger, H., Vapnik, Y., Banasik, K., Murashko, M., Agakhanov, A.A., and Pauluhn, A. (2019) Gmalimite, IMA 2019-007. CNMNC Newsletter No. 50; European Journal of Mineralogy, 31, 848.

García-Florentino, C., Torre-Fdez, I., Ruiz-Galende, P., Aramendia, J., Castro, K., Arana, G., Maguregui, M., Ortiz de Vallejuelo, S.F., and Madariaga, J.M. (2021) Development of innovative nondestructive analytical strategies for Mars Sample Return tested on Dar al Gani 735 Martian Meteorite. Talanta, 224, 121863.

Gross, S. (1970) The mineralogy of the Hatrurim Formation, Israel. Geological Survey of Israel Bulletin, 70, 1–80.

Haberle, C.W., and Garvie, L.A. (2017) Extraterrestrial formation of oldhamite and portlandite through thermal metamorphism of calcite in the Sutter's Mill carbonaceous chondrite. American Mineralogist, 102, 2415–2421.

Hammouda, T., Frossard, P., Boyet, M., Bouvier, A., Newville, M., and Lanzirotti, A. (2024) Mapping the redox state of the young Solar System using ytterbium valence state. Geochimica et Cosmochimica Acta, 372, 124–133.

394 Hunt, L., Stachel, T., McCandless, T.E., Armstrong, J., and Muelenbachs, K. (2012) Diamonds and
395 their mineral inclusions from the Renard kimberlites in Quebec. Lithos, 142, 267–284.
396 Ifantopulo, T.N., Yushko-Zakharova, O.E., Dubakina, L.S., and Shcherbachev, D.K. (1983)
397 Rasvumite from the Lovozero massif. Doklady Akademii Nauk SSSR, 269, 195–197 (in
398 Russian).
399 Jago, B.C., and Gittins, J. (1999) Mn- and F-bearing rasvumite in natrocarbonatite at Oldoinyo
400 Lengai volcano, Tanzania. Mineralogical Magazine, 63, 53–55.
401 Jamtveit, B., Dahlgren, S., and Austrheim, H. (1997) High-grade contact metamorphism of
402 calcareous rocks from the Oslo Rift, southern Norway. American Mineralogist, 82, 1241–
403 1254.
404 Johan, Z., Pierrot, R., and Schubnel, H.-J. (1970) La picotpaulite $TlFe_2S_3$, une nouvelle espèce
405 minérale. Bulletin de la Société française de Minéralogie et de Cristallographie, 93, 545–549
406 (in French).
407 Juroszek, R., Krüger, B., Galuskina, I., Krüger, H., Vapnik, Ye., and Galuskin, E. (2020) Siwaqaite,
408 $Ca_6Al_2(CrO_4)_3(OH)_{12}\cdot 26H_2O$, a new mineral of the ettringite group from the pyrometamorphic
409 Daba-Siwaqa complex, Jordan. American Mineralogist, 105, 409–421.
410 Klepp, K., and Boller, H. (1979) Die Kristallstruktur von $TlFeSe_2$ und $TlFeS_2$ (Synthetischer
411 Raguinit). Monatshefte für Chemie, 110, 1045–1055.
412 Konnert, J.A., and Evans, H.T. (1980) The crystal structure of erdite, $NaFeS_2\cdot 2H_2O$. American
413 Mineralogist, 65, 516–521.
414 Lafuente, B., Downs, R.T., Yang, H., and Stone, N. (2015) The power of databases: the RRUFF
415 project. In: Highlights in Mineralogical Crystallography, T. Armbruster and R.M. Danisi, eds.
416 Berlin, Germany, W. De Gruyter, pp 1-30.

Laurent, Y., Picot, P., Pierrot, R., and Ivanov, T. (1969) La raguinite, $TlFeS_2$, une nouvelle espèce minérale et le problème de l'allcharite. Bulletin de la Société française de Minéralogie et de Cristallographie, 92, 38–48 (in French).

Li, L., Gao, T., Ge, Y., Zhang, Q., Wang, J., Ma, Z., Guo, W., Yua, S., and Fan, Y. (2021) Ultra-long $KFeS_2$ nanowires grown on Fe foam as a high-performance anode for aqueous solid-state energy storage. Journal of Materials Chemistry A, 9, 27727–27735.

Ling, Z., and Wang, A. (2015) Spatial distributions of secondary minerals in the Martian meteorite MIL 03346,168 determined by Raman spectroscopic imaging. Journal of Geophysical Research - Planets, 120, 1141–1159.

Lisitsin, D.V., Dobrovol'skaya, M.G., Tsepin, A.I., Shcherbachev, D.K., Trubkin, N.V., and Kononkova, N.N. (2002) Sulfide mineralization in high-alkaline pegmatites of the Koashva deposit (Khibiny massif, Kola Peninsula). Geology of Ore Deposits, 44(5), 385–395.

Liu, Y., Chou, I.-M., Chen, J., Wu, N., Li, W., Bagas, L., Ren, M., Liu, Z., Mei, S., and Wang, L. (2023) Oldhamite: a new link in upper mantle for C-O-S-Ca cycles and an indicator for planetary habitability. National Science Review, 10, nwad159.

Logvinova, A.M., and Sharygin, I.S. (2023) Second natural occurrence of $KFeS_2$ (Hanswilkeite): an inclusion in diamond from the Udachnaya Kimberlite Pipe (Siberian Craton, Yakutia). Minerals, 2023, 13, 874.

Lorenz, C.A., Ivanova, M.A., Brandstaetter, F., Kononkova, N.N., and Zinovieva, N.G. (2020) Aubrite Pesyanoe: Clues to composition and evolution of the enstatite achondrite parent body. Meteoritics and Planetary Science, 55, 2670–2702.

Makreski, P., Jovanovski, G., and Boev, C. (2014) Micro-Raman spectra of extremely rare and endemic Tl-sulfosalts. Journal of Raman Spectroscopy, 45, 610–617.

Mitchell, R.H. (2006) Sylvite and fluorite microcrysts, and fluorite-nyerereite intergrowths from natrocarbonatite, Oldoinyo Lengai, Tanzania. Mineralogical Magazine, 70, 103–114.

Morgan, J. W., Czamanske, G. K., and Wandless, G. A. (1985) Origin and evolution of the alkalic ultramafic rocks in the Coyote Peak diatreme, Humboldt County, California. Geochimica et Cosmochimica Acta, 49, 749–760.

Nestola, F. (2023) Commentary on 'Oldhamite: a new link in upper mantle for C-O-S-Ca cycles and an indicator for planetary habitability'. National Science Review, 10, nwad185.

Novikov, I., Vapnik, Ye., and Safonova, I. (2013) Mud volcano origin of the Mottled Zone, Southern Levant. Geoscience Frontiers, 4, 597–619.

Osadchii, V.O., Voronin, M.V., and Baranov, A.V. (2018) Phase equilibria in the $KFeS_2$ – Fe – S system at 300 – 600 °C and bartonite stability. Contributions to Mineralogy and Petrology, 173, 44.

Oversby, V.M., and Ringwood, A.E. (1972) Potassium distribution between metal and silicate and its bearing on the occurrence of potassium in the core. Earth and Planetary Science Letters, 14, 345–347.

Panina, L.I., and Isakova, A.T. (2019) Djerfisherite in monticellite rocks of the Krestovskaya Intrusion (Polar Siberia). Petrology, 27, 171–185.

Pekov, I.V., Agakhanov, A.A., Boldyreva, M.M., and Grishin, V.G. (2005) Pautovite, $CsFe_2S_3$, a new mineral species form the Lovozero alkaline complex, Kola peninsula, Russia. Canadian Mineralogist, 43, 965–972.

Pouchou, J.L., and Pichoir, F. Quantitative analysis of homogeneous or stratified microvolumes applying the model BPAP. In Electron Probe Quantitation: Heinrich, K.F.J., Newbury, D.E., Eds.; Springer Verlag: New York, 1991.

Sharygin, V.V. (2022) Sodium-rich phosphate and silicate inclusions in the troilite nodule of the Darinskoe iron meteorite (IIC). Geochemistry International, 60, 1221–1236.

Sharygin, V.V., Kamenetsky, V.S., Kamenetskaya, M.B., Seretkin, Y.V., and Pokhilenko, N.P. (2007) Rasvumite from the Udachnaya-East pipe: The first finding in kimberlites. Doklady Earth Sciences, 415, 929–934.

Sharygin, V.V., Kamenetsky, V.S. and Kamenetsky, M.B. (2008) Potassium sulfides in kimberlite-hosted chloride-"nyerereite" and chloride clasts of Udachnaya-East pipe, Yakutia, Russia. Canadian Mineralogist, 46, 1079–1095.

Sheldrick, G.M. (2015) Crystal structure refinement with *SHELXL*. Acta Crystallographica, C71, 3–8.

Sokol, E.V., Deviatiiarova, A.S., Kokh, S.N., Reverdatto, V.V., Artemyev, D.A., and Kolobov, V.Y. (2019) Sulfide mineralization hosted by spurrite-mervinite marbles (Kochumdek River, East Siberia). Doklady Earth Sciences, 489, 1326–1329.

Sokolova, M.N., Dobrovol'skaya, M.G., Organova, N.I., Kazakova, M.E., and Dmitrik, A.L. (1970) Sulfide of potassium and iron – the new mineral rasvumite. Zapiski Vsesoyuznogo Mineralogicheskogo Obshchestva, 99, 712–720 (in Russian).

Sokolova, M.N., Dobrovol'skaya, M.G., Organova, N.I., Kazakova, M.E., and Vasil'eva, G.L. (1971) Find and distribution of djerfisherite in the Khibiny massif pegmatites. Geologiya Rudnikh Mestorozhdeniy, 13, 62–71 (in Russian).

Sorokhtina, N.V., Kogarko, L.N., Zaitsev, V.A., Kononkova, N.N., and Asavin, A.M. (2019) Sulfide mineralization in the carbonatites and phoscorites of the Guli massif, Polar Siberia, and their noble-metal potential. Geochemistry International, 57, 1125–1146.

Vapnik, Ye., Sharygin, V.V., Sokol, E.V., and Shagam, R. (2007) Paralavas in a combustion metamorphic complex: Hatrurim Basin, Israel. The Geological Society of America, Reviews in Engineering Geology, 18, 133–153.

Vereshchagin, O.S., Khmelnitskaya, M.O., Murashko, M.N., Shilovskikh, V.V., Vapnik, Ye., Zaitsev, A.N., Vlasenko, N.S., and Britvin, S.N. (2024) Reduced mineral assemblages of

superficial origin in west-central Jordan. Mineralogy and Petrology, 10.1007/s00710-024-00851-8

Wilke, H.-J. Mineral-Fundstellen, Band 4: Skandinavien. Christian Weise Verlag, Munich, 1976, 370 p.

Wilke, H.-J. Die Mineralien und Fundstellen von Schweden. Christian Weise Verlag, Munich, 1997, 200 p.

Wright, K., Critchley, P., and Garrard, A. (2008) Stone bead technologies and early craft specialization: insights from two Neolithic sites in eastern Jordan. Levant 40 (20), 131–165.

Yakovenchuk, V.N., Pakhomovsky, Y.A., Men'shikov, Y.P., Ivanyuk, G.Y.,Krivovichev, S.V., and Burns, P.C. (2003) Chlorbartonite, $K_6Fe_{24}S_{26}(Cl,S)$, a new mineral species from a hydrothermal vein in the Khibina massif, Kola peninsula, Russia: Description and crystal structure. Canadian Mineralogist, 41, 503–511.

503 **List of figure captions**

504

505 **Figure 1.** Hanswilkeite-bearing rock. (a) Freshly broken fragments of calcite-spurrite marble that
506 encases sulfide-bearing assemblages. (b) Polished marble plate. Black rock dissected by
507 hydrothermal calcite-jennite veinlets (Cal+Jnn), with numerous millimeters-sized grey cloudy
508 calcite nests containing late sulfides. The black color of the marble is imparted by the impregnations
509 of srebrodolskite, $Ca_2(Fe^{3+},Al)_2O_5$.

510

511 **Figure 2.** Hanswilkeite and its assemblages. (a) Purple hanswilkeite crystals disseminated within
512 calcite-silicate nest. Reflected light, crossed nicols. (b) Hanswilkeite grain surrounded by calcite
513 crystals. Reflected light. The upper-right corner is a view under crossed nicols, the bottom-left
514 corner is an image in parallel nicols. (c) White oldhamite crystals and scattered shiny red
515 hanswilkeite and pseudo-cubic red-brown srebrodolskite crystals in a calcite nest. Reflected light,
516 crossed nicols. (d) Purple hanswilkeite grains and yellowish euhedral pyrite crystals in calcite
517 matrix. Reflected light. Upper-right corner: parallel nicols; bottom-left one – crossed nicols.
518 Abbreviations: Hsw, hanswilkeite; Cal, calcite; Old, Oldhamite; Sre, srebrodolskite; Py, pyrite.

519

520 **Figure 3.** (a) Millimeter-sized, flame-colored hanswilkeite grain in a srebrodolskite-calcite nest.
521 Small round calcite crystals around the periphery of hanswilkeite. Reflected light; crossed nicols. (b)
522 Detail of a central part of the grain at higher magnification. The main matrix is hanswilkeite.
523 Reflected light. Tiny syntactic intergrowths of rasvumite, KFe_2S_3, are clearly visible as bluish-grey
524 patches under crossed nicols, becoming white under parallel nicols. (c) Reflectance curves of
525 hanswilkeite measured in air. Abbreviations: Hsw, hanswilkeite; Cal, calcite; Sre, srebrodolskite;
526 Rsv, rasvumite.

527

528 **Figure 4.** Raman spectrum of hanswilkeite. (a) The range between 1500 and 3800 cm^{-1} evidences
529 for the absence of O–H stretching vibrations. (b) The fingerprint region. The broad weak feature
530 between 550 and 750 cm^{-1} is probably caused by surface oxidation film on hanswilkeite polished
531 section. The intensity scale in (a) and (b) is the same.
532
533 **Figure 5.** Crystal structure of hanswilkeite. (a) General view, projection approximately onto {001}.
534 Infinite chains of edge-sharing tetrahedra [FeS_4] (yellow) propagated along the *c*-axis. Potassium
535 ions are shown as purple ellipsoids. (b) Fragment of a single chain of [FeS_4] tetrahedra,
536 corresponding to the stoichiometry of $[FeS_2]^-$ – the dithioferrate (III) anion. Drawn using ATOMS
537 6.1 software (Dowty 2006).
538
539 **Figure 6.** Crystal structures of hanswilkeite and related sulfides, in ellipsoid-and-stick
540 representation. (a) Hanswilkeite, $KFeS_2$ (this work): infinite chains of edge-sharing tetrahedra [FeS_4]
541 separated by K^+ ions. (b) Rasvumite, KFe_2S_3 (after Clark and Brown 1980): infinite ribbons $[Fe_2S_6]^{\infty}$
542 composed of doubled edge-sharing tetrahedra [FeS_4], charge-balanced by K^+ ions. (c) Erdite,
543 $NaFeS_2 \cdot 2H_2O$ (Konnert and Evans 1980). The same tetrahedral chains as in hanswilkeite, separated
544 by Na^+ ions and water molecules. (d) Raguinite, $TlFeS_2$ (Klepp and Boller 1979). The same chains
545 as in hanswilkeite, separated by Tl^+ ions. Legend: brown-red ellipsoids, Fe; yellow ones, S; violet,
546 K; deep-blue, Na; light-blue, oxygen; pale-green, Tl.
547
548
549
550
551
552

This is the peer-reviewed, final accepted version for American Mineralogist, published by the Mineralogical Society of America.
The published version is subject to change. Cite as Authors (Year) Title. American Mineralogist, in press.
DOI: https://doi.org/10.2138/am-2024-9494. http://www.minsocam.org/

Tables

Table 1. Reflectance data for hanswilkeite measured in air (%).

R_{max}	R_{min}	λ (nm)	R_{max}	R_{min}	λ (nm)
23.1	12.0	420	17.3	9.0	580
23.9	10.1	440	18.5	9.0	589 (COM) [a]
18.5	10.0	460	19.7	9.0	600
16.0	9.2	470 (COM) [a]	24.6	9.1	620
13.5	8.5	480	30.0	9.1	640
13.9	8.8	500	32.0	9.3	650 (COM) [a]
17.6	9.3	520	34.0	9.6	660
20.4	9.4	540	34.2	10.0	680
19.6	9.3	546 (COM) [a]	33.1	10.2	700
18.9	9.2	560			

[a] Reflectance values for four wavelengths required by Commission on Ore Mineralogy (COM)

Table 2. Chemical composition of hanswilkeite and associated rasvumite (wt. %).

	Hanswilkeite		**Rasvumite**	
	$n = 6$ [a]	Range	$n = 3$ [a]	Range
K	23.78	23.29 – 24.07	15.84	15.57 – 16.07
Rb	b.d.l. [b]		0.17	0.00 – 0.52
Ca	0.44	0.00 – 1.39	0.72	0.60 – 0.80
Fe	34.75	34.34 – 35.43	43.91	42.92 – 44.83
Mn	0.60	0.54 – 0.67	0.10	0.00 – 0.16
Zn	0.47	0.00 – 0.75	0.24	0.00 – 0.38
S	39.46	39.06 – 39.72	37.77	37.40 – 38.03
Total	**99.50**		**98.75**	

[a] Average of a given number of analyses. [b] b.d.l. – below detection limit.

This is the peer-reviewed, final accepted version for American Mineralogist, published by the Mineralogical Society of America.
The published version is subject to change. Cite as Authors (Year) Title. American Mineralogist, in press.
DOI: https://doi.org/10.2138/am-2024-9494. http://www.minsocam.org/

565

566 Table 3. X-ray powder diffraction data for hanswilkeite (d in Å) [a]

I_{meas}	d_{meas}	I_{calc}	d_{calc}	*hkl*	I_{meas}	d_{meas}	I_{calc}	d_{calc}	*hkl*
100	5.68	100	5.66	020	10	1.8796	12	1.8817	330
	5.64		5.65	110			4	1.8785	151
1	4.58	1	4.59	–111	2	1.8310	3	1.8308	–332
31	3.270	39	3.266	130	1	1.8140	3	1.8126	132
		5	3.256	200	4	1.7365	10	1.7360	–152
29	3.227	35	3.224	111	2	1.7049	7	1.7036	–402
45	2.921	57	2.919	–221	2	1.6831	6	1.6817	202
6	2.830	6	2.831	040	2	1.6512	3	1.6544	–313
		4	2.823	220			4	1.6509	–261
1	2.630	2	2.630	–112	3	1.6321	6	1.6328	260
12	2.510	15	2.511	131			3	1.6281	400
		5	2.508	–202	1	1.6067	1	1.6121	222
5	2.484	9	2.485	002	1	1.5891	5	1.5900	023
1	2.458	2	2.460	041	1	1.5677	5	1.5671	350
1	2.309	1	2.309	–311	1	1.5275	2	1.5290	–333
2	2.292	3	2.293	–222	1	1.5078	3	1.5081	–262
2	2.278	3	2.276	022	1	1.4586	2	1.4578	171
12	2.198	26	2.198	–132	1	1.4152	2	1.4154	080
4	2.138	2	2.139	150	1	1.3518	2	1.3530	421
		6	2.136	240			3	1.3516	–204
3	2.059	6	2.059	–312	1	1.3151	1	1.3159	–532

567

568 * Rigaku R-AXIS Rapid II diffractometer, semi-cylindrical imaging plate detector (r = 127.4
569 mm). Co$K\alpha$ radiation (λ = 1.79021 Å); rotating anode (40 kV, 15 μA) with microfocus
570 optics; Debye-Scherrer geometry, exposure time 60 min. Theoretical pattern was calculated
571 on the basis of atomic coordinates obtained from the structure refinement and unit-cell
572 parameters refined from powder diffraction data. Calculated intensities were normalized to
573 $\{I(020) + I(110)\}$ = 100. Calculated lines with intensity less than 1 have been omitted.
574

575

576

577

578
579
580 Table 4. Selected bond lengths (Å) in the crystal structure of hanswilkeite
581

Bond	Length	Bond	Length
K–S	3.3087(12) ×2	Fe–S	2.2394(12) ×2
K–S	3.4327(12) ×2	Fe–S	2.2304(12) ×2
K–S	3.4814(19) ×2	< Fe–S>	2.235
K–S	3.3462(19) ×2		
<K–S>	3.392	Fe–Fe	2.7007(2) ×2

582
583

584

585 Table 5. Comparative crystallographic data for hanswilkeite, its synthetic analogue and related
586 minerals
587

	Hanswilkeite	Synthetic	Rasvumite	Raguinite	Erdite
Formula	$KFeS_2$	$KFeS_2$	KFe_2S_3	$TlFeS_2$	$NaFeS_2 \cdot 2H_2O$
Crystal system	Monoclinic	Monoclinic	Orthorhombic	Monoclinic	Monoclinic
Space group	*C*2/*c*	*C*2/*c*	*Cmcm*	*C*2/*m*	*C*2/*c*
a (Å)	7.091	7.084	9.049	11.636	10.693
b (Å)	11.315	11.303	11.019	5.304	9.115
c (Å)	5.399	5.394	5.431	6.799	5.507
β (°)	113.2	113.2		116.7	92.2
V (Å^3)	398.1	397.0	541.5	374.8	536.4
Z	4	4	4	4	4
Reference	This work	Bronger et al. (1987)	Clark and Brown (1980)	Klepp and Boller (1979)	Konnert and Evans (1980)

588
589
590

This is the peer-reviewed, final accepted version for American Mineralogist, published by the Mineralogical Society of America.
The published version is subject to change. Cite as Authors (Year) Title. American Mineralogist, in press.
DOI: https://doi.org/10.2138/am-2024-9494. http://www.minsocam.org/

591
592 **Figures**

593

594

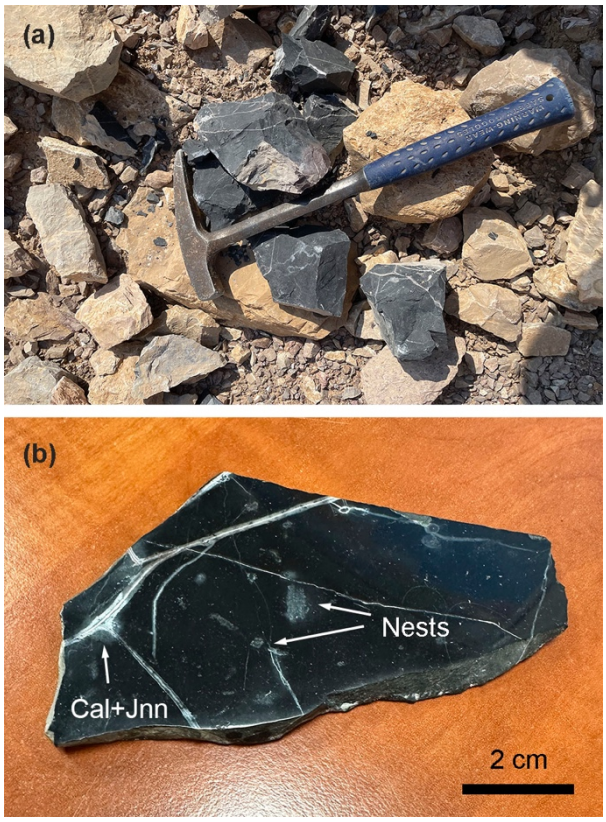

595

596 **Figure 1.** Hanswilkeite-bearing rock. (a) Freshly broken black fragments of calcite-
597 spurrite marble that encases sulfide-bearing assemblages and tan-colored fragments
598 of the same but weathered marble. (b) Polished marble plate. Black rock dissected by
599 hydrothermal calcite-jennite veinlets (Cal+Jnn), with numerous millimeters-sized
600 grey cloudy calcite nests containing late sulfides. The black color of the marble is
601 imparted by the impregnations of srebrodolskite, $Ca_2(Fe^{3+},Al)_2O_5$.
602

603

604

This is the peer-reviewed, final accepted version for American Mineralogist, published by the Mineralogical Society of America.
The published version is subject to change. Cite as Authors (Year) Title. American Mineralogist, in press.
DOI: https://doi.org/10.2138/am-2024-9494. http://www.minsocam.org/

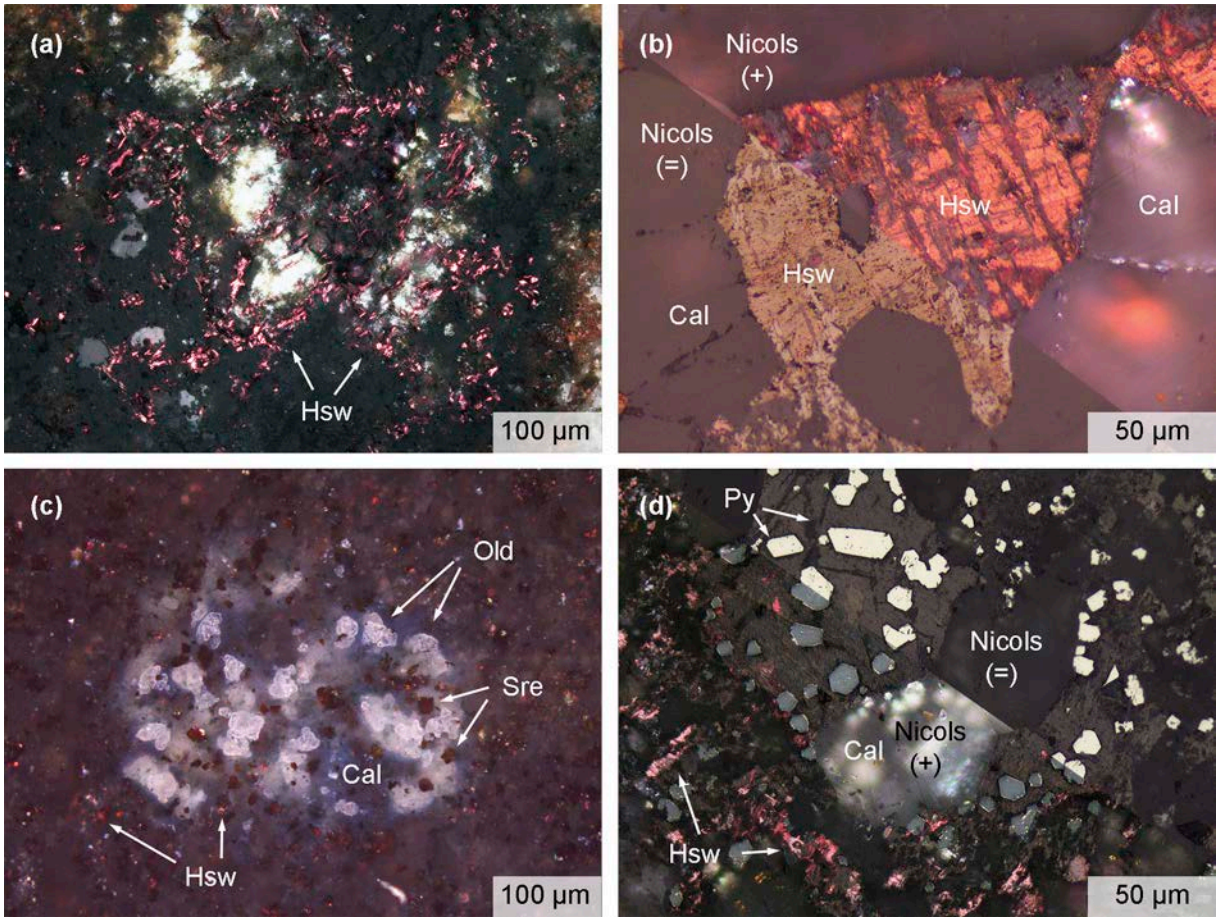

Figure 2. Hanswilkeite and its assemblages. (a) Purple hanswilkeite crystals disseminated within calcite-silicate nest. Reflected light, crossed nicols. (b) Hanswilkeite grain surrounded by calcite crystals. Reflected light. The upper-right corner is a view under crossed nicols, the bottom-left corner is an image in parallel nicols. (c) White oldhamite crystals and scattered shiny red hanswilkeite and pseudo-cubic red-brown srebrodolskite crystals in a calcite nest. Reflected light, crossed nicols. (d) Purple hanswilkeite grains and yellowish euhedral pyrite crystals in calcite matrix. Reflected light. Upper-right corner: parallel nicols; bottom-left one – crossed nicols. Abbreviations: Hsw, hanswilkeite; Cal, calcite; Old, Oldhamite; Sre, srebrodolskite; Py, pyrite.

This is the peer-reviewed, final accepted version for American Mineralogist, published by the Mineralogical Society of America.
The published version is subject to change. Cite as Authors (Year) Title. American Mineralogist, in press.
DOI: https://doi.org/10.2138/am-2024-9494. http://www.minsocam.org/

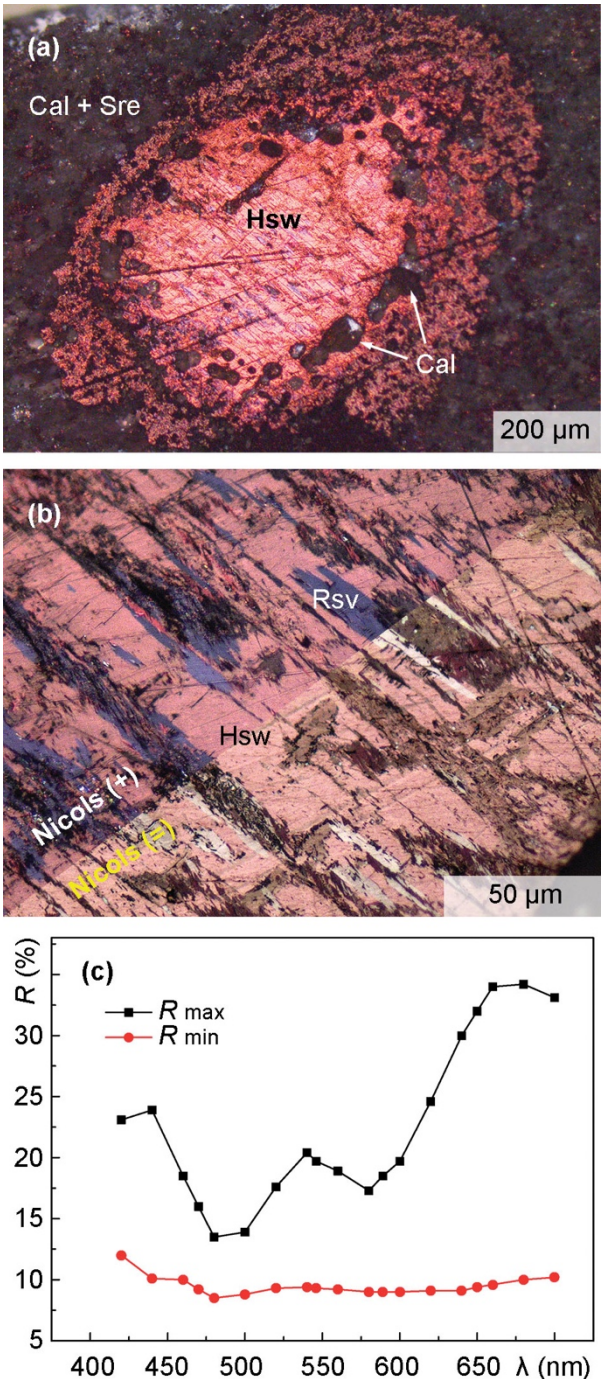

Figure 3. (a) Millimeter-sized, flame-colored hanswilkeite grain in a srebrodolskite-calcite nest. Small round calcite crystals around the periphery of hanswilkeite. Reflected light; crossed nicols. (b) Detail of a central part of the grain at higher magnification. The main matrix is hanswilkeite. Reflected light. Tiny syntactic intergrowths of rasvumite, KFe_2S_3, are clearly visible as bluish-grey patches under crossed nicols, becoming white under parallel nicols. (c) Reflectance curves of hanswilkeite measured in air. Abbreviations: Hsw, hanswilkeite; Cal, calcite; Sre, srebrodolskite; Rsv, rasvumite.

This is the peer-reviewed, final accepted version for American Mineralogist, published by the Mineralogical Society of America.
The published version is subject to change. Cite as Authors (Year) Title. American Mineralogist, in press.
DOI: https://doi.org/10.2138/am-2024-9494. http://www.minsocam.org/

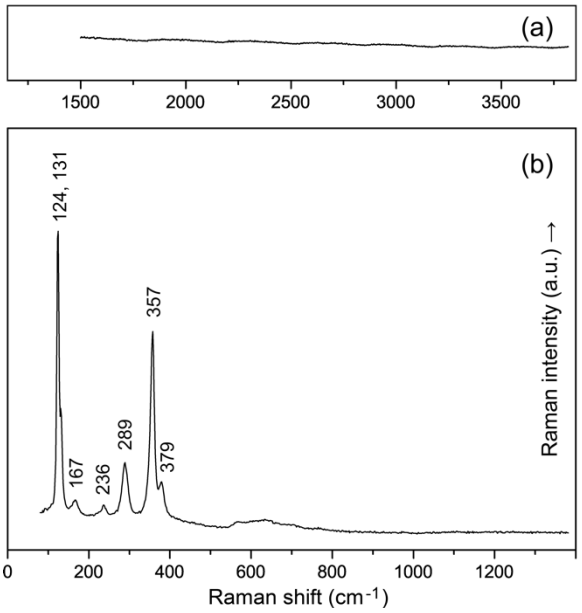

Figure 4. Raman spectrum of hanswilkeite. (a) The range between 1500 and 3800 cm^{-1} evidences for the absence of O–H stretching vibrations. (b) The fingerprint region. The broad weak feature between 550 and 750 cm^{-1} is probably caused by surface oxidation film on hanswilkeite polished section. The intensity scale in (a) and (b) is the same.

This is the peer-reviewed, final accepted version for American Mineralogist, published by the Mineralogical Society of America.
The published version is subject to change. Cite as Authors (Year) Title. American Mineralogist, in press.
DOI: https://doi.org/10.2138/am-2024-9494. http://www.minsocam.org/

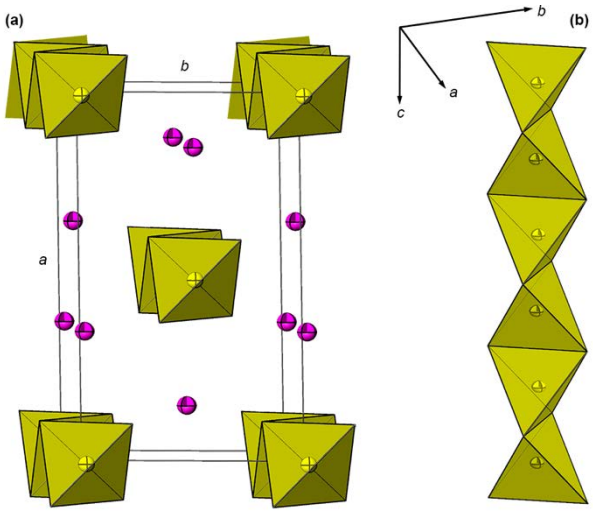

Figure 5. Crystal structure of hanswilkeite. (a) General view, projection approximately onto {001}. Infinite chains of edge-sharing tetrahedra [FeS_4] (yellow) propagated along the *c*-axis. Potassium ions are shown as purple ellipsoids. (b) Fragment of a single chain of [FeS_4] tetrahedra, corresponding to the stoichiometry of $[FeS_2]^-$ – the dithioferrate (III) anion. Drawn using ATOMS 6.1 software (Dowty 2006).

This is the peer-reviewed, final accepted version for American Mineralogist, published by the Mineralogical Society of America.
The published version is subject to change. Cite as Authors (Year) Title. American Mineralogist, in press.
DOI: https://doi.org/10.2138/am-2024-9494. http://www.minsocam.org/

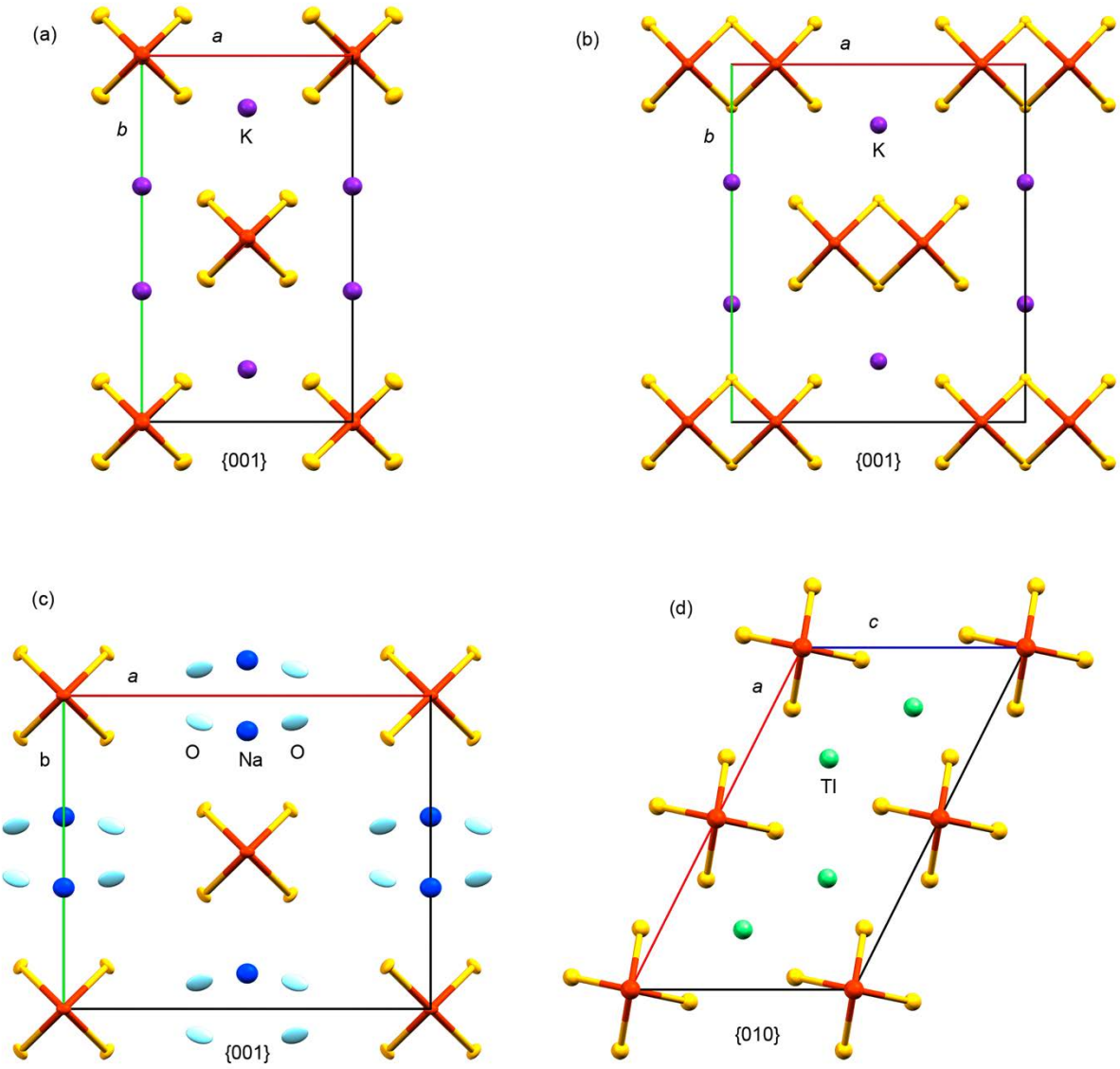

Figure 6. Crystal structures of hanswilkeite and related sulfides, in ellipsoid-and-stick representation. (a) Hanswilkeite, $KFeS_2$ (this work): infinite chains of edge-sharing tetrahedra $[FeS_4]$ separated by K^+ ions. (b) Rasvumite, KFe_2S_3 (after Clark and Brown 1980): infinite ribbons $[Fe_2S_6]^{\infty}$ composed of doubled edge-sharing tetrahedra $[FeS_4]$, charge-balanced by K^+ ions. (c) Erdite, $NaFeS_2 \cdot 2H_2O$ (Konnert and Evans 1980). The same tetrahedral chains as in hanswilkeite, separated by Na^+ ions and water molecules. (d) Raguinite, $TlFeS_2$ (Klepp and Boller 1979). The same chains as in hanswilkeite, separated by Tl^+ ions. Legend: brown-red ellipsoids, Fe; yellow ones, S; violet, K; deep-blue, Na; light-blue, oxygen; pale-green, Tl.